Bayesian Model Selection in Nonlinear Subspace Identification

Bayesian Model Selection in Nonlinear Subspace Identification

Rui Zhu, Qingguo Fei,

Southeast University, Nanjing, Jiangsu Province, 211189, China

Dong Jiang,

Nanjing Forestry University, Nanjing, Jiangsu Province, 210037, China

S. Marchesiello, D. Anastasio

Politecnico di Torino, Torino, 10129, Italy

https://doi.org/10.2514/1.J060782

Cite as:

R. Zhu, Q. Fei, D. Jiang, S. Marchesiello, D. Anastasio, Bayesian Model Selection in Nonlinear Subspace Identification, AIAA Journal 0 0:0, 1-10. doi: 10.2514/1.J060782

Bayesian Model Selection in Nonlinear Subspace Identification

Rui Zhu [1], and Qingguo Fei [2]
Southeast University, Nanjing, Jiangsu Province, 211189*, China*

Dong Jiang [3],
Nanjing Forestry University, Nanjing, Jiangsu Province, 210037*, China*

S. Marchesiello [4], and D. Anastasio [5]
Politecnico di Torino, Torino, 10121, Italy

Abstract: In nonlinear system identification, one of the main challenges is how to select a nonlinear model. The accuracy of nonlinear subspace identification depends on the accuracy of the nonlinear feedback force that the user chooses. Considering the uncertainties in the selection process of an appropriate nonlinear model, a novel Bayesian probability method calculation framework based on response data is established to improve the accuracy of nonlinear subspace identification. Three implementation steps are introduced: (*i*) establish candidate model database; (*ii*) the reconstructed signal can be calculated by nonlinear subspace identification; (*iii*) The posterior probability of each candidate model is estimated to get the optimal nonlinear model and determine the nonlinear coefficients of the nonlinearities. Two numerical simulations are investigated: a two-degrees of freedom spring-mass system with nonlinear damping and a cantilever beam with nonlinear stiffness. The influence of the noise on the robustness of the algorithm is considered. The experimental investigation is eventually undertaken considering a device showing elastic and damping nonlinearities. The latter is represented by a friction model depending on both velocity and displacement. Results indicate that the proposed approach can effectively identify the nonlinear system behavior with high accuracy.

---

[1] Ph.D. Candidate, School of Mechanical Engineering, rzhu@seu.edu.cn

[2] Professor, School of Mechanical Engineering, **Corresponding author**, qgfei@seu.edu.cn.

[3] Associate professor, School of Mechanical and Electronic Engineering, jiangdong@njfu.edu.cn.

[4] Professor, Dipartimento di Ingegneria Meccanica ed Aerospaziale, stefano.marchesiello@polito.it

[5] Postdoc researcher, Dipartimento di Ingegneria Meccanica ed Aerospaziale, dario.anastasio@polito.it

Nomenclature

(Nomenclature entries should have the units identified)

$f(t)$ = external force

f_n = nonlinear force

$\boldsymbol{h}$ = frequency response function

K = stiffness matrix

k_i = i_{th} spring stiffness

M = mass matrix

N = the number of the dimensional of freedom

$P(\mu_i)$ = prior plausibility of i_{th} candidate model

q = number of nonlinearity constituents

S = number of candidate models

μ_i = i_{th} candidate model

ω = angular frequency

w = displacement

α = nonlinear damping coefficient

Φ = data set from the measured information

I. Introduction

Nonlinear characteristics are common in aerospace structures. Accurate models [1][2] are essential to the research and application of aerospace engineering. System identification [3][4] is an efficient tool to determine the characteristics of both linear [5] and nonlinear systems. The latter case is becoming more important nowadays, as many engineering structures behave nonlinearly to some extent [6]. For some nonlinear identification methods, the nonlinear system cannot be regarded as a black box system, unlike the linear system identification [7]. The nonlinear characteristics need to be known in advance because the nonlinear system identification is affected by the accuracy of alternative model selection.

In the past decades, system identification methods of nonlinear structures have been reviewed [8][9]. The progress realized over that period is mainly highlighted, for instance, on accurate modeling and robust identification of joints interfacing subcomponents. Among the available methods, Marchesiello and Garibaldi [10] proposed the nonlinear subspace identification (NSI) approach and opened up new horizons to identify nonlinear mechanical systems due to the robustness and efficacy of the subspace approach. In Ref.[11], the clearance-type nonlinearity is successfully identified by NSI, where this method has better computational efficiency compared with the traditional polynomial method. In Ref. [12], a Duffing oscillator is identified by NSI under different excitation conditions. From the perspective of the frequency domain, Noël and Kerschen [13] developed a frequency-domain identification algorithm for nonlinear systems by using subspace theory. Taking a SmallSat spacecraft in practical engineering as the object, Noël et al. [14] carried out experimental research, and successfully identified the nonlinear characteristics of the joint by using the NSI in the time domain and frequency domain. More recently, the impact of spurious poles [15] has been investigated in NSI, and Marchesiello et al. introduced several modal decoupling tools. This allowed to identify the modal contributions of physical poles, significantly improving the estimation of the system parameters. The nonlinear subspace method has been also extended to the reduced-order domain [16], identifying the geometric nonlinear characteristic of a thin beam. Zhang et al. [17] developed an identification strategy for nonlinear parameter identification based on reconstructed signals and curve fitting adopting stepped sine experiments under constant excitation. The method has been also applied to a strongly nonlinear rotor-bearing system [18] to verify its performances in a practical engineering case. Singh and Moore [19] presented the characteristic nonlinear system identification approach, where the clearance nonlinearities of a system can be identified by the signal response under impulse excitation. Zhu et al. 0 proposed the hybrid approach based on a combination of NSI with the restoring force surface approach. This method not only can identify nonlinear stiffness but also determine nonlinear damping.

The above identification methods need to know the type of nonlinearity in advance. Therefore, model selection is of vital importance in the nonlinear identification strategy. Testing the accuracy of the candidate model description of the recognition structure is regarded as the standard of model selection. At present, there is no unique method for selecting the proper nonlinear model, and the choice is generally made case-by-case, depending on the characteristics of the specific identification problem. Due to the lack of understanding of the structure system to be identified, an improper selection of the identification parameters often occurs. Multiple different models can be

obtained, leading to the imperfect description of the structure to be identified. To find a reasonable model, it is therefore mandatory to develop a model selection approach to judge the model and its parameters. In system identification, the search the optimal model is generally performed among a series of candidate models. Considering the uncertainty in the process of model selection, the model selection method based on Bayesian theory can investigate the influence of multiple models on structural response prediction at the same time. It can also automatically limit the complex models and quantitatively calculate the probability of selecting each model. Among the possible candidate models, the most likely model can be selected based on the evidence obtained by the Bayesian method. The evidence equation can comprehensively take into account two factors: the complexity of the model and the data fitting ability. In Ref. [21], Green applied the annealing algorithm to the Bayesian system identification, which can avoid local trapping, so that the optimal model can be determined effectively and the computational cost can be reduced. Through the analysis of experimental data, the most reasonable hysteretic model of CLT connection is determined by the Bayesian approach [22].

In this paper, the idea of Bayesian model selection is adopted in the nonlinear subspace method. The candidate models are identified by the nonlinear subspace identification approach. By calculating each model selection probability evidence expression, the calculation framework of the model selection method based on Bayesian theory is established. The rest of this paper's outline is as follows: Section II. A introduces the Bayesian model selection. Section II. B presents the nonlinear subspace identification method. How to apply Bayesian model selection in NSI is described in Section II. C. Section III. A investigates the numerical simulation of a two-degree-of-freedom nonlinear system with nonlinear damping. The cantilever beam with unknown nonlinear stiffness is discussed in Sect. III.B. Section. IV presents an experimental study. The conclusions are drawn in Sect. V.

II. Theory

A. Bayesian model selection

The uncertainty of the model can be evaluated quantitatively by Bayesian inference. There are two main functions: model selection and parameter identification. This paper mainly uses the function of model selection to select the best model from all kinds of candidate models.

As known, the most credible model is related to the highest probability of occurrence under the condition of existing data due to Bayesian inference. Φ represents the data set from the measured information. μ_i represents the

i_{th} (i=1,2,…, S) candidate model. S represents the number of possible models. Based on the probability analysis method, the probability of occurrence of each model can be calculated quantitatively, and then the most likely model μ^* can be determined. The probability $P(\mu_i|\Phi)$ of the model can be calculated by

$$P(\mu_i \mid \Phi) = \frac{P(\Phi \mid \mu_i) P(\mu_i)}{\sum_{i=1}^{S} P(\Phi \mid \mu_i) P(\mu_i)},\ i=1,2,...,S \tag{1}$$

where $P(\Phi|\mu_i)$ represents model evidence based on the data Φ; $P(\mu_i)$ is the initial probability set based on reasonable judgment as a prior plausibility, with $\sum_{i=1}^{S} P(\mu_i) = 1$. In the absence of prior information, it is usually assumed that each candidate model has the same prior probability

$$P(\mu_i) = \frac{1}{S} \tag{2}$$

Based on the selected particular model, the corresponding new response signal can be reconstructed. Due to the influence of model error, there must be an error between reconstructed signal Y_t^i and original signal f_t^i.

$$Y_t^i = f_t^i + \varepsilon_t^i \tag{3}$$

where t is time; ε_t^i is the reconstitution error.

The likelihood function $P(\Phi|\mu_i)$ reflects the fitting degree of the model to the test data, which can be further calculated by

$$\begin{aligned} P(\Phi \mid \mu_i) &= \prod_{t=1}^{n} \frac{1}{\sqrt{2\pi}\sigma} \exp\left\{ -\frac{1}{2\sigma^2} \left[Y_t^i - f_t^i \right]^2 \right\} \\ &= \frac{1}{\left(\sqrt{2\pi}\sigma\right)^n} \exp\left\{ -\frac{1}{2\sigma^2} \left[Y_t^i - f_t^i \right]^2 \right\} \end{aligned} \tag{4}$$

B. Nonlinear subspace method

A nonlinear system can be expressed [13] as

$$M\ddot{w}(t) + C_v \dot{w}(t) + Kw(t) + f_n\left(w(t), \dot{w}(t)\right) = f(t) \tag{5}$$

where the mass matrix is represented by M, the linear stiffness matrix is denoted by K, the viscous damping matrix is expressed by C_v and the external force is represented by $f(t)$. f_n is the nonlinear force depending on displacement or velocity, which is regarded as a set of internal feedback forces. In this case, the nonlinear system is composed of

the internal feedback force and the underlying linear system as the linear part of the nonlinear system. Based on the nonlinear characteristics and components, the nonlinear force can be rewritten by:

$$f_n\left(w(t),\dot{w}(t)\right)=\sum_{i=1}^{q}\lambda_i l_i n_i\left(w,\dot{w}\right) \tag{6}$$

where Eq.(6) has q nonlinearity constituents, the vector l_i represents the information about the location of the i^{th} nonlinearity. The scalar function $n_i(t)$ represents the mathematical function expression of the i^{th} nonlinearity, which can be a nonlinear stiffness or nonlinear damping, λ_i is the scalar identified nonlinear parameter for the i^{th} nonlinear component.

By bringing Eq.(6) into Eq.(5), one can obtain

$$M\ddot{w}(t)+C_v\dot{w}(t)+Kw(t)=f(t)-\sum_{i=1}^{q}\lambda_i l_i n_i\left(w,\dot{w}\right) \tag{7}$$

Based on the state-space equation concept, the identity $\dot{w}=\dot{w}$ is combined with Eq.(7). The state-space formulation can be obtained by:

$$\begin{Bmatrix}\dot{w}\\ \ddot{w}\end{Bmatrix}=\begin{bmatrix}0_{N\times N} & I_{N\times N}\\ -M^{-1}K & -M^{-1}C\end{bmatrix}\begin{Bmatrix}w\\ \dot{w}\end{Bmatrix}+\begin{bmatrix}0_{N\times N} & 0_{N\times 1} & \text{L} & 0_{N\times 1}\\ M^{-1} & M^{-1}\lambda_1 l_1 & \text{L} & M^{-1}\lambda_q l_q\end{bmatrix}\begin{Bmatrix}f(t)\\ -n_1(t)\\ \text{M}\\ -n_q(t)\end{Bmatrix} \tag{8}$$

$$y=\begin{bmatrix}I_{N\times N} & 0_{N\times N}\end{bmatrix}\begin{Bmatrix}w\\ \dot{w}\end{Bmatrix}+\begin{bmatrix}0_{N\times N} & 0_{N\times 1} & \text{L} & 0_{N\times 1}\end{bmatrix}\begin{Bmatrix}f(t)\\ -n_1(t)\\ \text{M}\\ -n_q(t)\end{Bmatrix} \tag{9}$$

where the state vector $\begin{bmatrix}w & \dot{w}\end{bmatrix}^T$ can be expressed as x, and the output response is represented by vector y. I represents the identity matrix. Therefore, a continuous state-space model is used to describe the nonlinear system above.

$$\begin{aligned}\dot{x}&=A_c x+B_c u\\ \dot{y}&=Cx+Du\end{aligned} \tag{10}$$

where the dynamical system matrix is represented by A_c, the input matrix is indicated by B_c, the output matrix is expressed as C, and the direct feedthrough matrix is stated by D. u is the extended input vector [10].

$$A_c=\begin{bmatrix}0 & I\\ -M^{-1}K & -M^{-1}C\end{bmatrix} \tag{11}$$

$$B_c = \begin{bmatrix} 0_{N\times N} & 0_{N\times 1} & \mathrm{L} & 0_{N\times 1} \\ M^{-1} & M^{-1}\lambda_1 l_1 & \mathrm{L} & M^{-1}\lambda_q l_q \end{bmatrix} \tag{12}$$

$$C = \begin{bmatrix} I_{N\times N} & 0_{N\times N} \end{bmatrix} \tag{13}$$

$$D = \begin{bmatrix} 0_{N\times N} & 0_{N\times 1} & \mathrm{L} & 0_{N\times 1} \end{bmatrix} \tag{14}$$

$$u = \begin{bmatrix} f(t) & -n_1(t) & \mathrm{L} & -n_q(t) \end{bmatrix}^T \tag{15}$$

The discrete state vector can be defined as $x_r = x(r\Delta t)$. And the sampling period is expressed as Δt. Therefore，Eq.(10) can be translated into a discrete state-space model to analyze the discrete signal in the actual measurement.

$$\begin{aligned} x_{r+1} &= Ax_r + Bu_r \\ y_r &= Cx_r + Du_r \end{aligned} \tag{16}$$

where the dynamical system matrix A can be obtained by

$$A = e^{A_c \Delta t} \tag{17}$$

The input matrix B is

$$B = \left(e^{A_c \Delta t} - I\right) A_c^{-1} B_c \tag{18}$$

The identification process of NSI is briefly described. The subspace identification problem includes estimating the model order n and the system matrices. The input Hankel matrix $W_{0\backslash 2i\text{-}1}$ can be expressed as

$$W_{0\backslash 2i-1} \overset{def}{=} \left[\begin{array}{cccc} w(0) & w(1) & \mathrm{L} & w(l-1) \\ w(1) & w(2) & \mathrm{L} & w(l) \\ \mathrm{M} & \mathrm{M} & \mathrm{O} & \mathrm{M} \\ w(i-1) & w(i) & \mathrm{L} & w(i+l-2) \\ \hline w(i) & w(i+1) & \mathrm{L} & w(i+l-1) \\ w(i+1) & w(i+2) & \mathrm{L} & w(i+l) \\ \mathrm{M} & \mathrm{M} & \mathrm{O} & \mathrm{M} \\ w(2i-1) & w(2i) & \mathrm{L} & w(2i+l-2) \end{array}\right] \overset{def}{=} \left[\begin{array}{c} W_p \\ \hline W_r \end{array}\right] \tag{19}$$

where the “past” and “future” signal is described by the subscript p and f, respectively. The index i represents the number of block rows. The output block matrix $O_{0\backslash 2i\text{-}1}$ has the same expression as $W_{0\backslash 2i\text{-}1}$. Based on Eq.(16), the relationship between input and output can be expressed as

$$\begin{bmatrix} O(0) \\ O(1) \\ O(2) \\ \mathrm{M} \\ O(i-1) \end{bmatrix} = \begin{bmatrix} C \\ CA \\ CA^2 \\ \mathrm{M} \\ CA^{i-1} \end{bmatrix} x_0 + \underbrace{\begin{bmatrix} D & 0 & 0 & 0 & 0 \\ CB & D & 0 & 0 & 0 \\ CAB & CB & D & 0 & 0 \\ \mathrm{M} & & \mathrm{O} & \mathrm{O} & 0 \\ CA^{i-2}B & CA^{i-3}B & \mathrm{L} & CB & D \end{bmatrix}}_{G_i} \begin{bmatrix} w(0) \\ w(1) \\ w(2) \\ \mathrm{M} \\ w(i-1) \end{bmatrix} \tag{20}$$

where Γ_i is the extended observability matrix and G_i is the lower triangular Toeplitz matrix.

$$\Gamma_i = \begin{bmatrix} C & CA & CA^2 & \mathrm{L} & CA^{i-1} \end{bmatrix}^T \tag{21}$$

Then, the matrix O_f can be divided into linear combinations of the two non-orthogonal matrices W_f and Z_p and of the orthogonal complement of W_f and Z_p:

$$O_f = L_{U_f} W_f + L_{Z_p} Z_p + L_{W_f^{\perp}, Z_p^{\perp}} \begin{pmatrix} O_f \\ Z_p \end{pmatrix}^{\perp} \tag{22}$$

where the orthogonal complement can be represented by the symbol $\perp$. The computation of these terms above and their geometric interpretations are introduced in Ref.[23]. The matrix $L_{Zp}Z_p$ is the oblique projection of the row space of O_f along the row space of W_f on the row space of Z_p, which can be expressed as the symbol $\vartheta_i = O_f \,/_{W_f} Z_p$. Then, the singular value decomposition (SVD) of the following weighted oblique projection is performed:

$$\vartheta_i \Pi_{W_f^{\perp}} = WSV^T = \begin{bmatrix} W_1 & W_2 \end{bmatrix} \begin{bmatrix} S_1 & 0 \\ 0 & S_2 \end{bmatrix} \begin{bmatrix} V_1^T \\ V_2^T \end{bmatrix} \tag{23}$$

where $\Pi_{W_f^{\perp}}$ is the projection on the orthogonal complement of the row space of the W_f. The model order n can be confirmed by checking the singular value. Then, the extended observability matrix can be obtained by $\Gamma_i = W_i S_i^{1/2}$ based on Eq.(23). The matrices A and C can be estimated by Eq.(21). Then, the matrix B and D can be solved in Eq.(20) based on the least square method [23].

Due to the existence of nonlinearity, the "extended" frequency response function (FRF) matrix is expressed as

$$\boldsymbol{H}_E(\omega) = \boldsymbol{D} + \boldsymbol{C}\left(j\omega \boldsymbol{I} - \boldsymbol{A}_c\right)^{-1} \boldsymbol{B}_c \tag{24}$$

where ω is the circular frequency. The underlying linear system FRF $\boldsymbol{H}$ can be defined as

$$\boldsymbol{H}(\omega) = \left(K + j\omega C_v - \omega^2 M\right)^{-1} \tag{25}$$

By defining

$$\boldsymbol{Q} = j\omega\boldsymbol{I} - \boldsymbol{A}_c = \begin{bmatrix} \boldsymbol{Q}_{11} & \boldsymbol{Q}_{12} \\ \boldsymbol{Q}_{21} & \boldsymbol{Q}_{22} \end{bmatrix} \tag{26}$$

the corresponding inverse matrix can be expressed as

$$\boldsymbol{R} = \left(j\omega\boldsymbol{I} - \boldsymbol{A}_c\right)^{-1} = \begin{bmatrix} \boldsymbol{R}_{11} & \boldsymbol{R}_{12} \\ \boldsymbol{R}_{21} & \boldsymbol{R}_{22} \end{bmatrix} \tag{27}$$

By substituting Eq.(27) into (24), one can obtain

$$\begin{aligned} \boldsymbol{H}_E(\omega) &= \boldsymbol{0} + \begin{bmatrix} \boldsymbol{I} & \boldsymbol{0} \end{bmatrix} \begin{bmatrix} \boldsymbol{R}_{11} & \boldsymbol{R}_{12} \\ \boldsymbol{R}_{21} & \boldsymbol{R}_{22} \end{bmatrix} \begin{bmatrix} \boldsymbol{0} & \boldsymbol{0} & \mathrm{L} & \boldsymbol{0} \\ \boldsymbol{M}^{-1} & \boldsymbol{M}^{-1}\lambda_1 V_1 & \mathrm{L} & \boldsymbol{M}^{-1}\lambda_r V_r \end{bmatrix} \\ &= \boldsymbol{R}_{12}\boldsymbol{M}^{-1} \begin{bmatrix} \boldsymbol{I} & \lambda_1 V_1 & \mathrm{L} & \lambda_r V_r \end{bmatrix} \end{aligned} \tag{28}$$

where $\boldsymbol{R}_{12}$ can be calculated adopting the block matrix inversion rule.

$$\boldsymbol{R}_{12} = -\boldsymbol{Q}_{11}^{-1}\boldsymbol{Q}_{12}\boldsymbol{J}_{Q_{11}}^{-1} \tag{29}$$

$$\boldsymbol{J}_{Q_{11}}^{-1} = \left(\boldsymbol{Q}_{22} - \boldsymbol{Q}_{21}\boldsymbol{Q}_{11}^{-1}\boldsymbol{Q}_{12}\right) \tag{30}$$

Then, $\boldsymbol{R}_{12}$ can be expressed as

$$\boldsymbol{R}_{12} = = \frac{1}{j\omega}\left(\boldsymbol{M}^{-1}C_d + j\omega\boldsymbol{I} + \boldsymbol{M}^{-1}K\frac{1}{j\omega}\right)^{-1} \tag{31}$$

Finally, Eq.(24) can be expressed as

$$\boldsymbol{H}_E(\omega) = \begin{bmatrix} \boldsymbol{H} & \boldsymbol{H}\lambda_1 V_1 & \mathrm{L} & \boldsymbol{H}\lambda_r V_r \end{bmatrix} \tag{32}$$

where the relationship of the "extended" FRF $\boldsymbol{H}_E$ and the underlying linear system FRF $\boldsymbol{H}$ can be established.

Due to the existence of the imaginary part j in Eq.(24), the nonlinear coefficients determined by $\boldsymbol{H}_E(\omega)$ are complex and frequency-dependent quantities, whose real parts converge to their exact values. The imaginary parts are theoretically null, but the presence of noise and nonlinear modeling errors can lead to non-zero imaginary parts in practice.

C. The framework of Bayesian model selection in NSI

In the nonlinear subspace identification problem, the prior nonlinear characterization accuracy has a vital role in determining whether the recognition result is good or bad. In practical engineering, the nonlinear characteristics of a structure might be difficult to determine directly. To solve this problem, NSI takes advantage of the Bayesian model selection skillfully in the presented approach. The flowchart of the proposed approach is shown in **Fig. 1**, where

three detailed steps are introduced. **Step 1**: Based on engineering experience and prediction, all possible nonlinear models are selected as the candidate model database ***S***; **Step 2**: For any candidate model, the same data is used to obtain the associated nonlinear parameters and the identified system matrices by NSI. The corresponding reconstructed signal can be calculated. The response signals are brought into Eq.(4) and Eq.(5), and the model evidence $P(\Phi|\mu_i)$ can be obtained; **Step 3**: The posterior probability of each candidate model is calculated to get the optimal nonlinear model and determine the nonlinear coefficients of the nonlinearities.

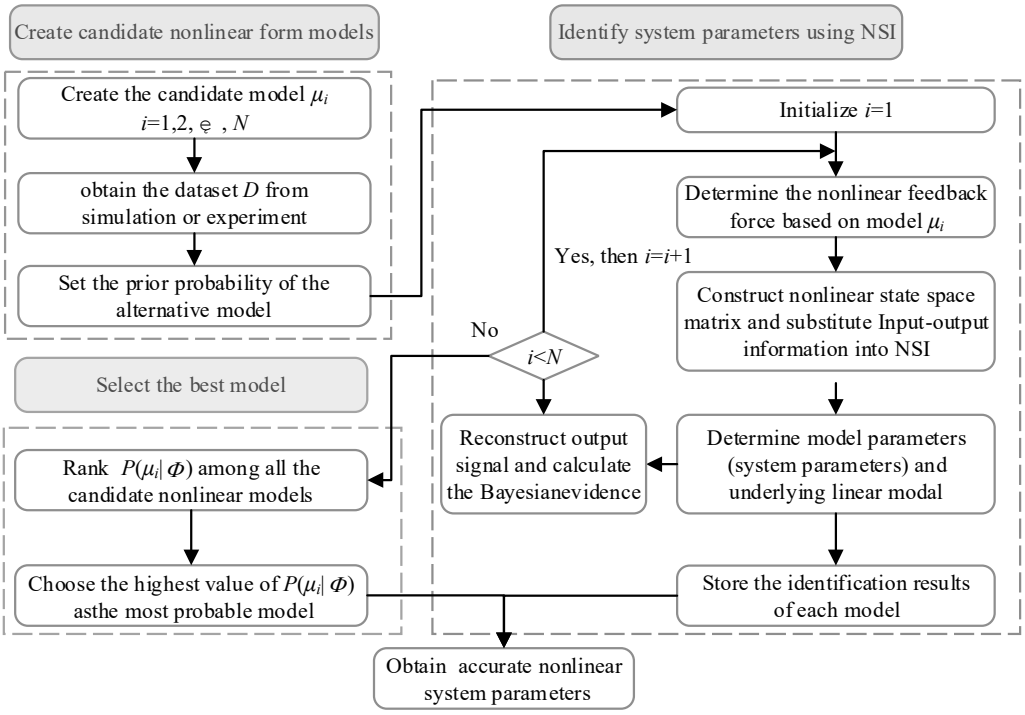

Fig. 1 Flowchart of the nonlinear subspace method with the Bayesian model selection

III. Numerical simulation

Two numerical simulations are conducted to demonstrate the proposed method's performances: a Two-DOF spring-mass system with quadratic friction and a cantilever beam with nonlinear stiffness.

A. Two degrees of freedom system with nonlinear damping

Fig. 2 shows the two-degree-of-freedom system with nonlinear damping. Quadratic friction is located at DOF 1. The parameters of the system are listed in **Table 1**.

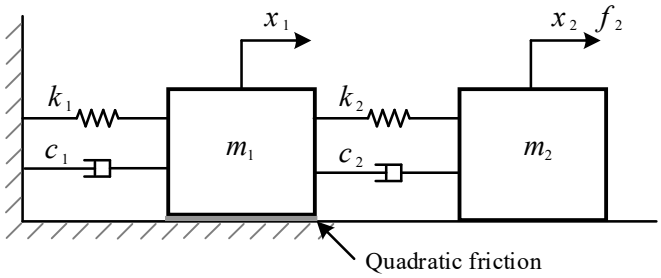

Fig. 2 A two-degrees of freedom spring-mass system with Quadratic friction

Table 1 System parameters of 2-DOFs

Mass (kg)	Linear stiffness (N/m)	Damping (Ns/m)	Nonlinear damping (Ns^2/m^2)
m_1=1	k_1=800	c_1=2	α=20
m_2=1.5	k_2=1000	c_2=2	

It is assumed that the nonlinear damping form is unknown. **Table 2** provides three standard friction models: Model 1 is the Quadratic friction; Model 2 represents Coulomb friction; Model 3 illustrates a combination of Model 1 and Model 2. Each candidate model has the same prior probability $P(\mu_i)$=1/3 based on Eq.(3).

Table 2 Information on candidate models

No	Model description	Function form	$P(\mu_i)$
Model 1: μ_1	quadratic friction	$\alpha_1 \dot{x}\lvert\dot{x}\rvert$	1/3
Model 2: μ_2	Coulomb friction	$\alpha_2 Sgn(\dot{x})$	1/3
Model 3: μ_3	quadratic friction and Coulomb friction	$\alpha_1 \dot{x}\lvert\dot{x}\rvert + \alpha_2 Sgn(\dot{x})$	1/3

A zero-mean Gaussian random force is selected to be applied at DOF 2, whose root-mean-square value is 10 N. Fourth-order Runge-Kutta approach is used to calculate the vibration response, with a sampling frequency of 100 Hz and acquisition length of 10s. As known, adverse noise can pollute the measured signals. To investigate the robustness of the method above, zero-mean Gaussian noise is imposed on the simulation signal in the 2% of the signal standard deviation.

Take the candidate Model 1 for example: the singular value plot can be calculated by NSI as shown in **Fig. 3**. Through the characteristic of abrupt change of the curve, the model order of the system is determined as n=4.

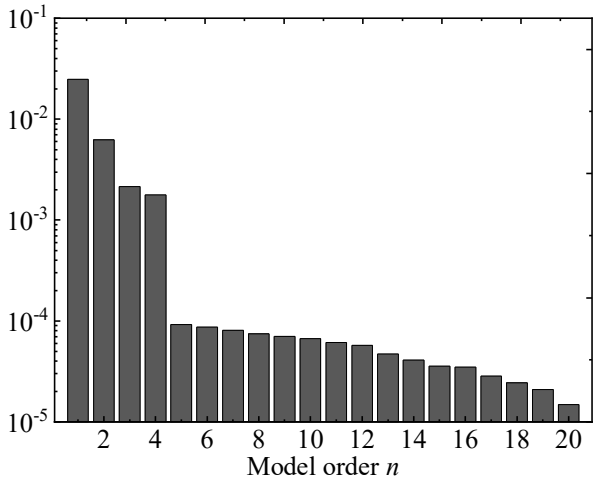

Fig. 3 Singular value plot with 2% measurement error considering quadratic friction

As shown in **Fig. 4**, the underlying FRF h_{12} based on candidate models is obtained by NSI. The identified modal parameters are presented in **Table 3**. Results show that: (1) The identified underlying FRFs are reasonably consistent with the exact values when Model 1 is selected; (2) In Model 2 or Model 3, the curve of the identified FRFs deviates from each other around the fundamental frequencies. This phenomenon reflects that the selected model does not match the true damping characteristic; (3) Though the noise exists, the maximum error of damping in Model 1 is only 5.49%, while the maximum error is two orders of magnitude higher in other cases. Therefore, the damping model of the system should be quadratic friction (Model 1).

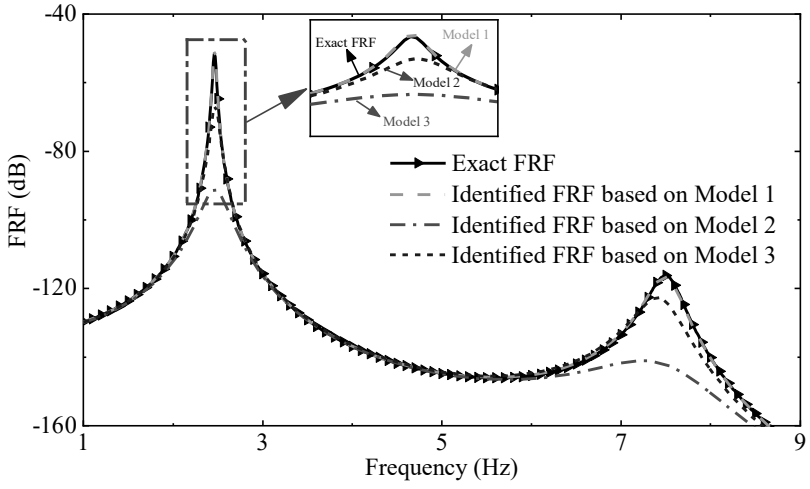

Fig. 4 Underlying linear FRF of different candidate models

Table 3 Identified model parameters of candidate models

Underlying linear system	Exact value	Model 1		Model 2		Model 3	
		Identified	Error/%	Identified	Error/%	Identified	Error/%
1st frequency/Hz	2.46	2.46	-0.02	2.47	0.46	2.47	0.46
2nd frequency/Hz	7.51	7.50	-0.13	7.48	-0.47	7.44	-0.97
1st damping ratio/%	0.91	0.86	-5.49	6.67	633.05	1.97	116.39
2nd damping ratio/%	2.53	2.58	1.89	9.43	272.69	3.61	42.68

The identified nonlinear parameters of each model are listed in **Table 4**. For each candidate model, the reconstructed response signal can be obtained from the identified state-space matrices. The corresponding posterior probability is calculated by Eq.(1) and Eq.(4). The posterior probability of Model 1 is mostly 100%, and one of the other candidate models is zero. The corresponding nonlinear parameter identification error of Model 1 is only 2.5%, even in the presence of noise. The results of other models can not represent the structure nonlinear characteristics, and they have no significance compared with the theoretical value.

Table 4 Identified nonlinear parameters and posterior probability of candidate models

	Exact value	Model 1		Model 2		Model 3	
		Identified	Error/%	Identified	Error/%	Identified	Error/%
quadratic friction: α_1	20.00	20.5	2.5	--	--	16.07	19.6
Coulomb friction: α_2	--	--	--	-0.72	--	-0.172	
$P(\mu_i \mid \Phi)$/%	--	100		0		0	

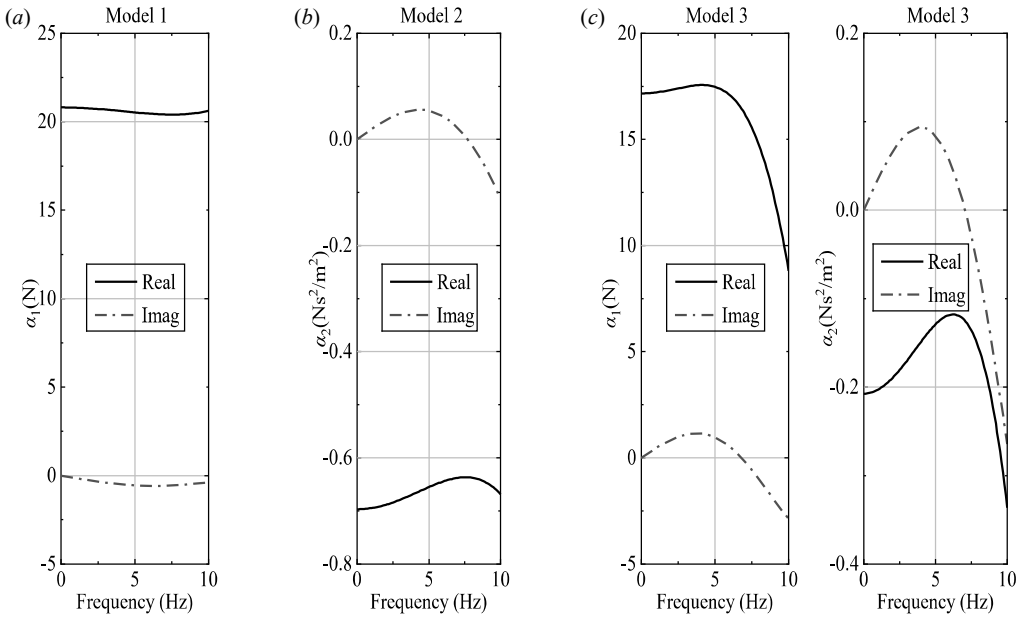

Fig. 5 Real and imaginary parts of the identified coefficients with noise for different candidate models

Meanwhile, the nonlinear coefficients identified by NSI are shown in **Fig. 5** for different candidate Models. The real part of the coefficient of Model 1 is several orders of magnitude higher than the imaginary part, which is not always the case for the other models. Results prove that Model 1 is the optimal model. The proposed method is effective without knowing a priori the exact nonlinear characteristics. This method can select the nonlinear model and has the capability of accurate identification.

B. Cantilever beam with nonlinear stiffness

In this section, a cantilever beam with nonlinear stiffness is discussed. In **Fig. 6**, the length of the beam is l = 50 cm, and it is divided into eight units with a total of 16 degrees of freedom. The density of the system is ρ = 1.2 g/cm^3, and the modulus of elasticity is $E = 7\times10^7$ GPa. The cross-section of a beam is circular and the size is 5 cm^2. There exists a nonlinear stiffness at DOF 13 as following:

$$k_n = k_2 x_{13}^{\ 2} + k_3 x_{13}^{\ 3} \tag{33}$$

where $k_2 = 8\times10^4$ N/m^2 is the square nonlinear coefficient, and the cubic nonlinear coefficient is represented by $k_3 = 4\times10^6$ N/m^3.

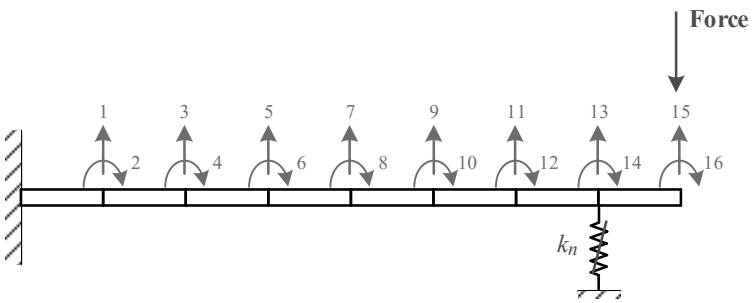

Fig. 6 A cantilever beam with nonlinear stiffness.

It is assumed that the nonlinear stiffness form is unknown. **Table 5** provides three nonlinear models: Each candidate model has the same prior probability $P(\mu_i)$ =1/3 based on Eq.(3).

Table 5 Information on candidate models

No	Model description	Function form	$P(\mu_i)$
Model 1: μ_1	square stiffness	$k_2x^2\cdot\text{sign}(x)$	1/3
Model 2: μ_2	cubic stiffness	k_3x^3	1/3
Model 3: μ_3	square stiffness and cubic stiffness	$k_2x^2+k_3x^3$	1/3

A zero-mean Gaussian random force is selected to be applied at DOF 15. The root-mean-square value is 10 N. The dynamical system response is calculated by applying the Runge-Kutta fourth-order method, with a sampling frequency of 1000 Hz and acquisition length of 100s. 1% noise is added in the signal.

Take the candidate Model 3 for example, and the singular value plot can be calculated by NSI as shown in **Fig. 7**. Through the characteristic of abrupt change of the curve, the model order of the system is determined as n=32.

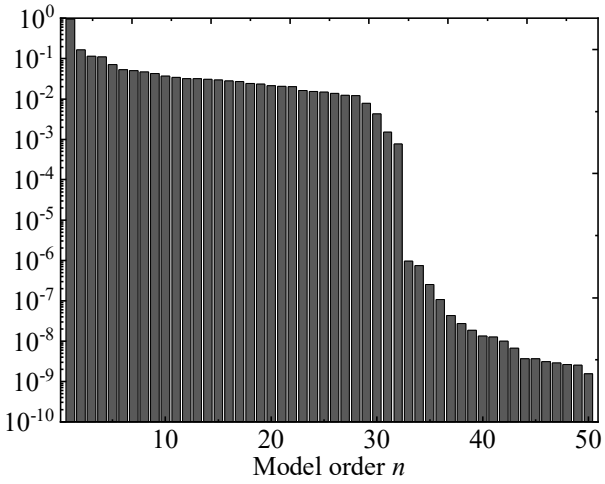

Fig. 7 Singular value plot of Model 3

As shown in **Fig. 8**, the underlying FRFs $h_{13,15}$ based on candidate models are obtained by NSI. The identified model parameters are shown in **Table 6**. Results show that: (1) The determined underlying FRF curve of Model 1 has a significant deviation from the theoretical value, and the first-order natural frequency is missing; (2) When the candidate Model 2 is considered, the amplitude of the curve deviates completely; (3) The identified underlying FRF are reasonably consistent with the exact value when the Model 3 is selected. The max error of natural frequency is only 0.23%. Therefore, the nonlinear stiffness model of the system should be quadratic stiffness and cubic stiffness (Model 3).

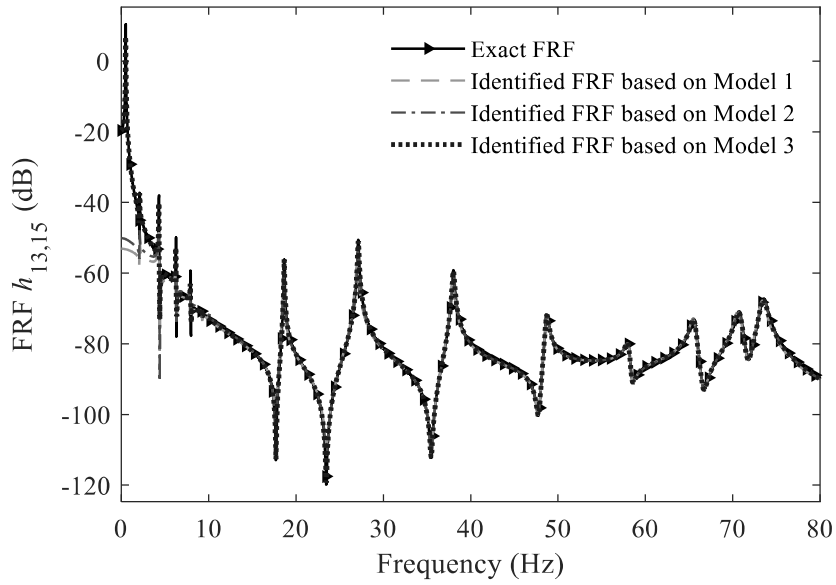

Fig. 8 Underlying linear FRF of different candidate models

Table 6 Identified modal parameters of candidate models

Model order	Exact value	Model 1		Model 2		Model 3	
		Identified	Error/%	Identified	Error/%	Identified	Error/%
1	0.509	--	--	--	--	0.508	-0.23
2	2.098	2.096	-0.10	2.205	5.10	2.098	-0.02
3	4.310	4.297	-0.28	4.318	0.21	4.309	0.02
4	6.266	6.117	-2.38	6.258	-0.12	6.265	0.01
5	7.934	7.815	-1.49	7.923	-0.13	7.933	0.00
6	9.221	9.008	-2.30	9.209	-0.13	9.221	-0.01
7	10.105	--	--	--	--	10.107	0.00
8	10.554	--	--	--		10.555	-0.01
9	18.648	15.205	-18.46	17.534	-5.97	18.648	0.05
10	27.132	25.961	-4.32	27.139	0.03	27.130	0.00

Identified nonlinear parameters of each model are shown in **Table 7**. For each candidate model, the reconstructed response signal can be obtained from the identified state-space matrices. The corresponding posterior probability is calculated by Eq.(1) and Eq.(4). The posterior probability of Model 3 is mostly 100%, and one of the other candidate models is zero. As proof, the time histories generated by NSI with the three models are presented and compared with the real response in **Fig. 9**. The error of the reconstructed sign based on Model 3 is almost zero, and other model errors are apparent. The corresponding nonlinear parameter identification error of Model 3 is only

0.75%. The results of other models can not represent the nonlinear characteristics of the structure. Results the proposed method can effectively determine the nonlinear stiffness model and nonlinear parameters.

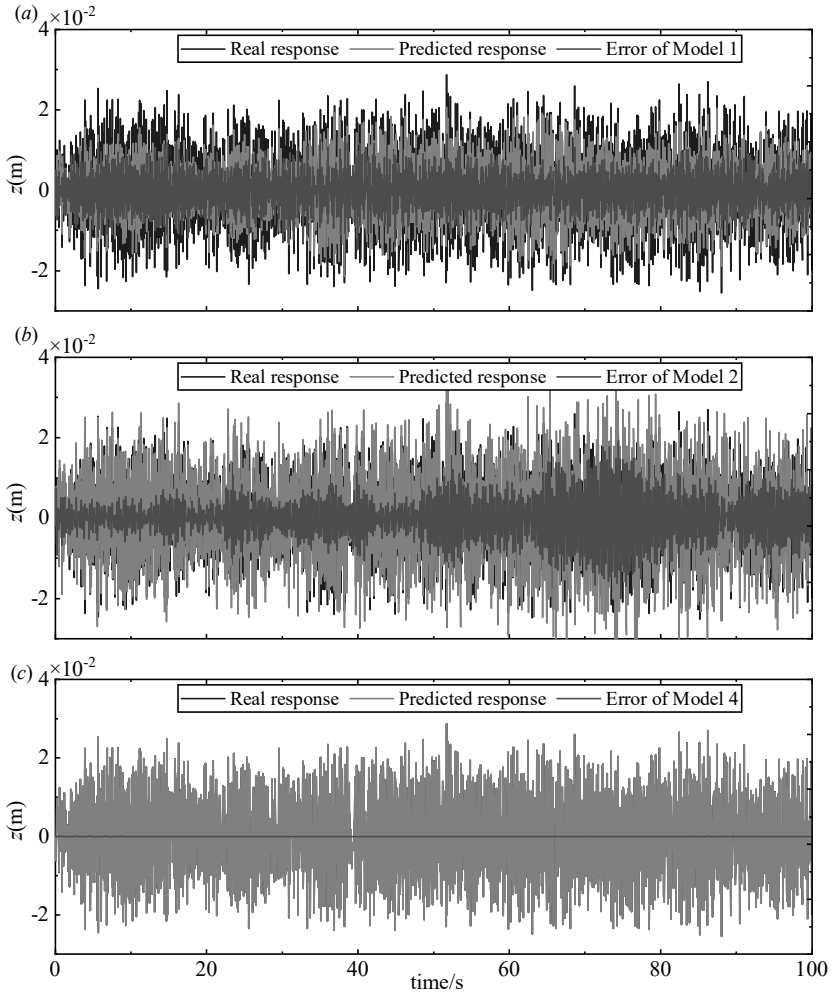

Fig. 9 Error of the time histories generated by NSI with three models

Table 7 Identified nonlinear parameters and posterior probability of candidate models

	Exact value	Model 1		Model 2		Model 3	
		Identified	Error/%	Identified	Error/%	Identified	Error/%
square stiffness：k_2	8.00×10^4	1.26×10^5	56.93	--	--	8.05×10^4	0.63
cubic stiffness：k_3	4.00×10^6	--	--	1.81×10^6	-54.68	4.03×10^6	0.75
$P(\mu_i\|\Phi)$/%	--	0		0		100	

IV. Experimental study

The experimental test of the negative system is conducted in Ref. [24]. The experimental photos are depicted in **Fig. 10**, showing the device's stable equilibrium positions. The device has negative stiffness characteristics and exhibits strong nonlinear behavior. The motion can be bounded around one of the two stable equilibrium positions, or it can be of cross-well type. Therefore, it can be regarded as a single degree of freedom system, considering the displacement of the moving central mass. The system is excited with a shaking table providing a random excitation. The sampling duration is t=140 s, and the sampling frequency is set to 512 Hz. The equilibrium positions are measured with a laser vibrometer, and they are equal to w_-^*=-0.0301m and w_+^*=0.0242m.

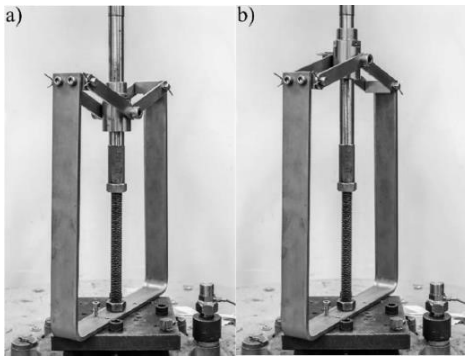

Fig. 10 Test picture of negative stiffness system [24]

As known reported in detail in [24], a new displacement variable $z(t)=w(t)-w^*$ can be defined when a negative reference position w^* is considered. In this case, the system is defined as a stable underlying linear system. Therefore, the equation of motion can be written by

$$m\ddot{z}+c\dot{z}+k_1 z+k_2 z^2+k_3 z^3+f_d=f(t) \tag{34}$$

where f_d is the nonlinear damping force. For this experimental system, the nonlinear damping form is challenging to determine a priori. Based on the experimental results in Ref.[25], the friction force in this negative stiffness oscillator depends on the position and velocity. Friction is related to normal force f_N, such as f_N*sign($\dot{w}$). Under these circumstances, the normal force is not constant but a function of the position w. Intuitively, the normal force is maximum at w_0^* when the rods are at their maximum compression, and minimum at $w_\pm^*$. Assuming that a quadratic function can describe this behavior. When $z(t)=w(t)-w^*$ is considered, the corresponding friction function can be written as follows:

$$f_d = \alpha_1 sign(\dot{x})\left(\beta z^2 + \gamma z + \delta\right) \tag{35}$$

where the three coefficients (β, γ, δ) related to two stable equilibrium positions $w_{\pm}^*$ are uniquely determined, and the only α_1 is the parameter to be identified.

$$\beta = \frac{1}{w_-^* w_+^*} \tag{36}$$

$$\gamma = \frac{2w^* - w_-^* - w_+^*}{w_-^* w_+^*} \tag{37}$$

$$\delta = 1 + \frac{w^*\left(w^* - w_-^* - w_+^*\right)}{w_-^* w_+^*} \tag{38}$$

Common friction forms, such as Coulomb friction and quadratic friction, are also considered in a real structure. Therefore, four candidate models are shown in **Table 8**. Each candidate model has the same prior probability $P(\mu_i)$=1/4 based on Eq.(3).

Table 8 Information on candidate models

No	Function form	$P(\mu_i)$
Model 1: μ_1	$\alpha_1 sign(\dot{x})\left(\beta z^2 + \gamma z + \delta\right)$	0.25
Model 2: μ_2	$\alpha_1 sign(\dot{x})\left(\beta z^2 + \gamma z + \delta\right) + \alpha_2 sign(\dot{x})\dot{x}^2$	0.25
Model 3: μ_3	$\alpha_1 sign(\dot{x})\left(\beta z^2 + \gamma z + \delta\right) + \alpha_3 sign(\dot{x})$	0.25
Model 4: μ_4	$\alpha_1 sign(\dot{x})\left(\beta z^2 + \gamma z + \delta\right) + \alpha_2 sign(\dot{x})\dot{x}^2 + \alpha_3 sign(\dot{x})$	0.25

Take the candidate Model 1 for example. The singular value plot can be calculated by NSI, as shown in **Fig. 11**. Through the characteristic of abrupt change of the curve, the model order of the underlying linear system is determined n=2.

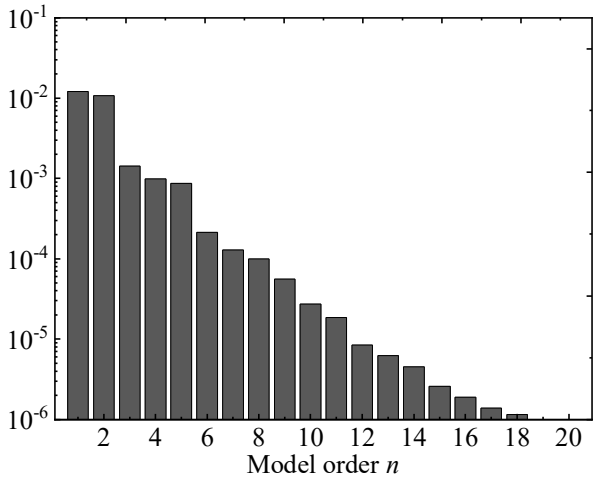

Fig. 11 Singular value plot of the candidate Model 1

For four candidate models, **Table 9** shows the modal parameter results of the underlying linear systems related to the negative reference value. Meanwhile, the proposed method's underlying estimated FRF h can be obtained, as shown in **Fig. 12**. Due to different friction models, damping identification values are quite different. It is difficult to determine the optimal result only based on NSI.

Table 9 Identified model parameters of candidate models in a negative position

	Model 1	Model 2	Model 3	Model 4
Natural frequency/Hz	11.64	11.40	11.84	11.51
Damping ratio/%	5.27	10.77	5.54	19.88

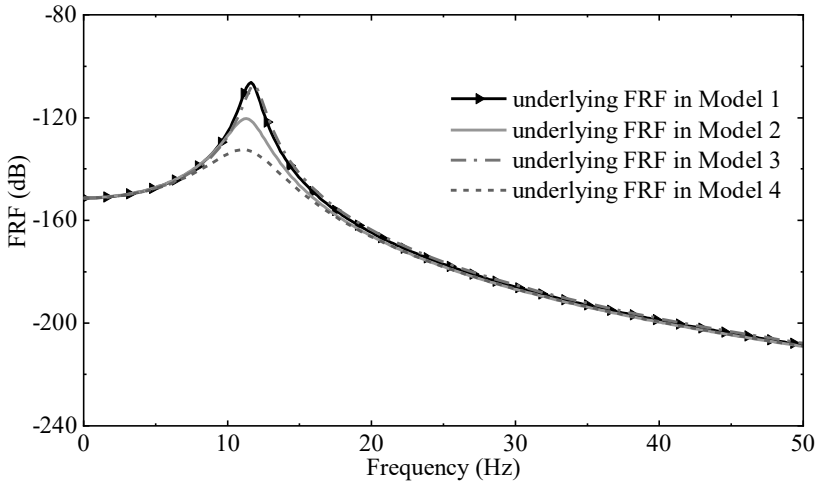

Fig. 12 Underlying linear FRF of different candidate models in the negative equilibrium position

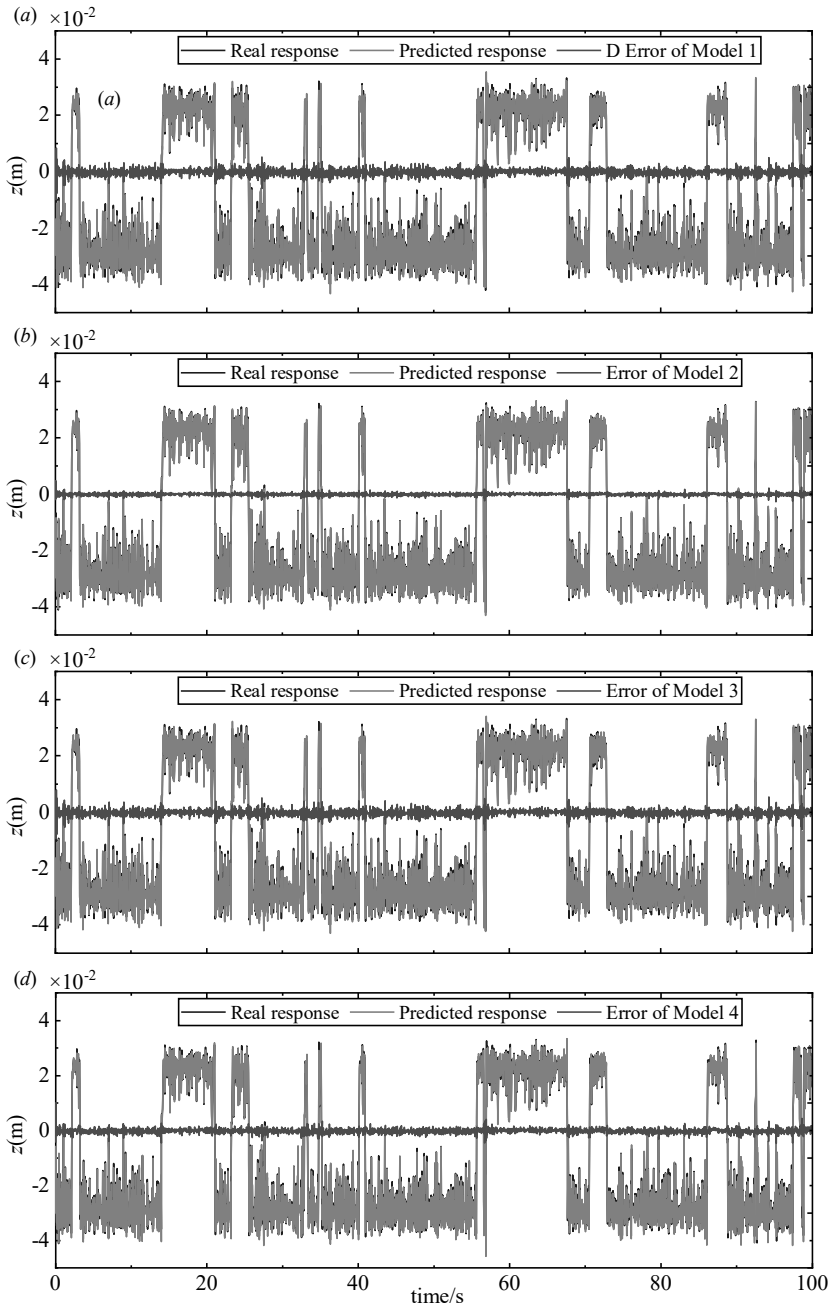

Fig. 13 Error of the time histories generated by NSI with four models

In this paper, the proposed method provides an effective way to determine the optimal structural model. Identified nonlinear parameters of each model are shown in **Table 10**. For each candidate model, the reconstructed response signal can be obtained. As proof, the time histories generated by NSI with the four models are presented

and compared with the true response in **Fig. 13**. The error of the reconstructed sign based on Model 2 is the smallest. The corresponding posterior probability is calculated by Eq.(1) and Eq.(4). Results show that the posterior probability of Model 2 is the largest, reaching 72.63%. Secondly, the posterior probability of model 4 is 27.35%. Therefore, the test system's optimal model is Model 2, and the friction is mainly composed of an ad-hoc friction model depending on velocity and displacement plus the standard quadratic friction.

Table 10 Identified nonlinear parameters and posterior probability of candidate models

Model order	Model 1	Model 2	Model 3	Model 4
	Identified	Identified	Identified	Identified
k_1 (N/m)	1.39×10^2	1.34×10^2	1.44×10^2	1.36×10^2
k_2 (N/m^2)	-6.04×10^4	-6.34×10^4	-6.22×10^4	-6.37×10^4
k_3 (N/m^3)	6.86×10^5	7.23×10^5	7.12×10^5	7.27×10^5
α_1 (N)	2.08	1.16	2.07	1.96
α_2 (Ns^2/m^2)	--	-4.61	--	-1.31
α_3 (N)	--	--	-0.05	-7.50
$P(\mu_i\|\Phi)$/%	0.01	72.63	0.01	27.35

The elastic restoring force of the system can be extracted from the experimental result based on the restoring force surface method and compared with the identified ones for the different nonlinear models, defined as:

$$R = k_3 z^3 + k_2 z^2 + k_1 z \tag{39}$$

The results of the comparison are depicted in **Fig. 14**. Results show that the agreement Model 2 is the highest among the candidate models, which verifies the proposed method's effectiveness.

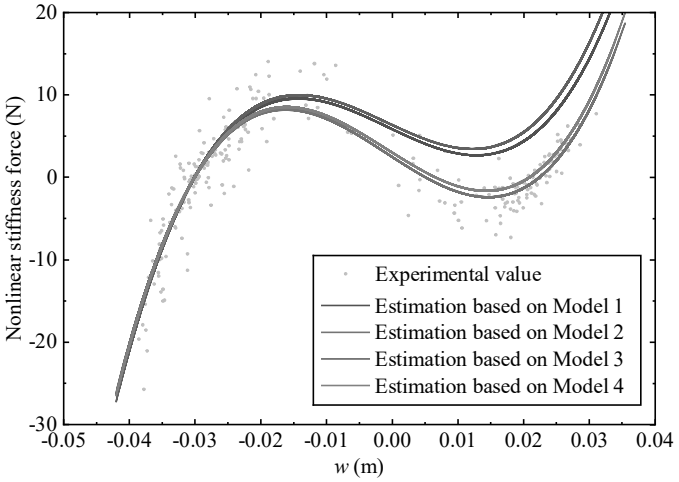

Fig. 14 Estimation of the restoring force

V. Conclusion

In this paper, Bayesian model selection is further applied to the nonlinear subspace identification approach. The remarkable feature of the presented methodology is that it accurately determines the most suitable nonlinear model generally unknown, and accurately identifies the nonlinear parameters. Simulation examples with unknown nonlinear damping or stiffness characteristics are conducted to verify the effectiveness in noisy conditions. An experimental study is eventually performed on a negative stiffness system, exhibiting rich nonlinear dynamics due to a combination of elastic and damping nonlinearities. The identified restoring force of the optimal candidate model estimated by the proposed approach is compared with the experimental restoring force values, showing a very high agreement. This testing application further proves the efficiency of the proposed method, which can be applied to various engineering structures exhibiting a nonlinear behavior.

Acknowledgments

This research work is supported by the National Natural Science Foundation of China (11602112 and 11572086), and the Scientific Research Foundation of the Graduate School of Southeast University (YBPY2003).

References

[1] Soize, C., Capiez-Lernout, E., and Ohayon, R., "Robust Updating of Uncertain Computational Models Using Experimental Modal Analysis," *AIAA Journal*, Vol.46, No. 11, 2018, pp. 2955-2965. https://doi.org./10.2514/1.38115

[2] Placzek, A., Tran, D.-M., and Ohayon, R., "A nonlinear POD-Galerkin Reduced-order Model for Compressible Flows Taking into Account Rigid Body Motions," *Computer Methods in Applied Mechanics and Engineering*, Vol.200, No.49-52, 2011, pp. 3497-3514. https://doi.org./10.1016/j.cma.2011.08.017

[3] Bagherzadeh, S., "Nonlinear Aircraft System Identification Using Artificial Neural Networks Enhanced by Empirical Mode Decomposition," *Aerospace Science and Technology*, Vol.75, 2018, pp.155-171. https://doi.org./10.1016/j.ast.2018.01.004

[4] Moore K. J., Mojahed, A., Bergman, L.A., and Vakakis, A.F., "Local Nonlinear Stores Induce Global Dynamical Effects in an Experimental Model Plane," *AIAA Journal*, Vol. 57, No. 11, 2019, pp. 4953-4965.

https://doi.org./10.2514/1.J058311

[5] Zhu, R., Fei, Q., Jiang, D., and Cao, Z., "Dynamic Sensitivity Analysis Based on Sherman–Morrison–Woodbury Formula," *AIAA Journal*, Vol. 57, No. 11, 2019, pp. 4992-5001.
https://doi.org./10.2514/1.J058280

[6] Jing, X.J., and Vakakis, A.F., "Exploring Nonlinear Benefits in Engineering," *Mechanical Systems and Signal Processing*, Vol.125, 2019, pp. 1-3.
https://doi.org./10.1016/j.ymssp.2019.01.059

[7] Zhu, R., Fei, Q., Jiang, D., and Cao, Z., "Removing Mass Loading Effects of Multi-transducers Using Sherman-Morrison-Woodbury formula in Modal Test," *Aerospace Science and Technology*, 2019. Vol. 93, pp. 105241.
https://doi.org./10.1016/j.ast.2019.06.022

[8] Kerschen, G., Worden, K., Vakakis, A.F., and Golinval, J.C., "Past, Present and Future of Nonlinear System Identification in Structural Dynamics," *Mechanical Systems and Signal Processing*, Vol. 20, No. 3, 2006, pp. 505-592.
https://doi.org./10.1016/j.ymssp.2005.04.008

[9] Noël, J.P., and Kerschen, G., "Nonlinear System Identification in Structural Dynamics: 10 More Years of Progress," *Mechanical Systems and Signal Processing*, Vol. 93, 2017, pp. 2-35.
https://doi.org./10.1016/j.ymssp.2016.07.020

[10] Marchesiello, S., and Garibaldi, L., "A Time Domain Approach for Identifying Nonlinear Vibrating Structures by Subspace Methods," *Mechanical Systems and Signal Processing*, Vol. 22, No. 1, 2008, pp. 81-101.
https://doi.org./10.1016/j.ymssp.2007.04.002

[11] Marchesiello, S., and Garibaldi, L., "Identification of Clearance-type Nonlinearities," *Mechanical Systems and Signal Processing*, Vol. 22, No. 5, 2008, pp. 1133-1145.
https://doi.org./10.1016/j.ymssp.2007.11.004

[12] Gandino, E., and Marchesiello, S., "Identification of a Duffing Oscillator under Different Types of Excitation," *Mathematical Problems in Engineering*, 2010, pp. 1-15.
https://doi.org./10.1155/2010/695025

[13] Noël, J.P., and Kerschen, G., "Frequency-domain Subspace Identification for Nonlinear Mechanical Systems," *Mechanical Systems and Signal Processing*, Vol. 40, No. 2, 2013, pp. 701-717.
https://doi.org./10.1007/978-1-4614-6570-6_8

[14] Noël, J.P., Marchesiello, S., and Kerschen, G., "Subspace-based Identification of a Nonlinear Spacecraft in the Time and Frequency Domains," *Mechanical Systems and Signal Processing*, Vol. 43, No. 2, 2014, pp. 217-236.
https://doi.org./10.1016/j.ymssp.2013.10.016

[15] Marchesiello, S., Fasana, A., and Garibaldi, L., "Modal Contributions and Effects of Spurious Poles in Nonlinear Subspace Identification," *Mechanical Systems and Signal Processing*, Vol. 74, 2016, pp. 111-132. https://doi.org./10.1016/j.ymssp.2015.05.008

[16] Anastasio, D., Marchesiello, S., Kerschen, G., and Noël, J.P., "Experimental Identification of Distributed Nonlinearities in the Modal Domain," *Journal of Sound and Vibration*, Vol. 458, 2019, pp. 426-444. https://doi.org./10.1016/j.jsv.2019.07.005

[17] Zhang, G., Zang, C., and Friswell, M.I., "Identification of Weak Nonlinearities in MDOF Systems Based on Reconstructed Constant Response Tests." *Archive of Applied Mechanics*, Vol. 89, No. 10, 2019, pp. 2053-2074. https://doi.org./10.1007/s00419-019-01559-4

[18] Zhang, G., Zang, C., and Friswell, M.I., "Parameter Identification of a Strongly Nonlinear Rotor-Bearing System Based on Reconstructed Constant Response Tests," *Journal of Engineering for Gas Turbines and Power*, Vol. 142, No. 8, 2020, pp. 081004 https://doi.org./10.1115/1.4047783

[19] Singh, A., and Moore, K.J., "Characteristic Nonlinear System Identification of Local Attachments with Clearance Nonlinearities," *Nonlinear Dynamics*, Vol. 102, No. 3, 2020, pp. 1-18. https://doi.org./10.1007/s11071-020-06004-8

[20] Zhu, R., Fei, Q., Jiang, D., and Cao, Z., Marchesiello, S., and Anastasio, D., "Identification of Nonlinear Stiffness and Damping Parameters Using a Hybrid Approach," *AIAA Journal*, 2021. https://doi.org/10.2514/1.J060461

[21] Green, P. L., "Bayesian System Identification of a Nonlinear Dynamical System Using a Novel variant of Simulated Annealing," *Mechanical Systems and Signal Processing*, Vol. 52-53, 2015, pp. 133-146. https://doi.org./10.1016/j.ymssp.2014.07.010

[22] Cao, J., Xiong, H., Zhang, F. L., Chen, L., and Cazador, CR., "Bayesian Model Selection for the Nonlinear Hysteretic Model of CLT Connections," *Engineering Structures*, Vol. 223, 2020, pp. 111118. https://doi.org./10.1016/j.engstruct.2020.111118

[23] Van Overschee, P., and De Moor, B., *Subspace Identification for Linear Systems: Theory-Implementation-Applications*, Kluwer Academic Publ., Dordrecht, The Netherlands, 1996, pp. 95–134. https://doi.org./10.1007/978-1-4613-0465-4

[24] Anastasio, D., Fasana, A., Garibaldi, L., and Marchesiello, S., "Nonlinear Dynamics of a Duffing-like Negative Stiffness Oscillator: Modeling and Experimental Characterization," *Shock Vibratio*n. Vol. 2020, 2020, pp. 1–13. https://doi.org./10.1155/2020/3593018

[25] Anastasio, D., and Marchesiello, S., “Experimental Characterization of Friction in a Negative Stiffness Nonlinear Oscillator,” *Vibration*, Vol. 3, No.2, 2020, pp. 132-148.
https://doi.org./10.3390/vibration3020011